DØnote 4573

Draft 3.1

Measurement of the Cross section for Inclusive Z Production in Di-muon Final States at $\sqrt{s} = 1.96$ TeV

The DØ Collaboration

(Dated: August 11, 2004)

A preliminary measurement of the cross section for the process $p\bar{p} \to Z/\gamma \to \mu^+\mu^-$ at $\sqrt{s} = 1.96$ TeV in the mass range $M > 40$ GeV is described. The measurement is performed using a data sample corresponding to an integrated luminosity of 148 pb^{-1} collected at the Fermilab Tevatron with the DØ detector between September 2002 and October 2003. A total of 14352 di-muon events are selected with an estimated background fraction of $(0.5 \pm 0.3)\%$ arising from $b\bar{b}$, $(0.1 \pm 0.1)\%$ from cosmic rays, $(0.5 \pm 0.1)\%$ from $Z \to \tau^+\tau^-$ and $(0.2 \pm 0.1)\%$ from $W \to \mu\nu$ and di-boson backgrounds. The result is

$$\sigma(p\bar{p} \to Z/\gamma \to \mu^+\mu^-) = 329.2 \pm 3.4(\text{stat.}) \pm 7.8(\text{syst.}) \pm 21.4(\text{lumi.}) \text{ pb}$$

Correcting the number of di-muon events by a factor of 0.885 ± 0.015 for the contribution from pure photon exchange and Z/γ interference, the result

$$\sigma(p\bar{p} \to Z \to \mu^+\mu^-) = 291.3 \pm 3.0(\text{stat.}) \pm 6.9(\text{syst.}) \pm 18.9(\text{lumi.}) \text{ pb}$$

is obtained.

I. INTRODUCTION

A measurement of the cross section for the process $p\bar{p} \rightarrow Z/\gamma \rightarrow \mu^+\mu^-$ at $\sqrt{s}$=1.96 TeV for propagator masses greater than 40 GeV is described below. The value of the cross section for $p\bar{p} \rightarrow Z/\gamma \rightarrow \mu^+\mu^-$ is evaluated using the following formula:

$$\sigma(p\bar{p} \rightarrow Z/\gamma \rightarrow \mu^+\mu^-) = \frac{N_{\rm cand}(1 - f_{\rm bb} - f_{cosmic})(1 - f_{\tau\tau})(1 - f_{W\rightarrow\mu\nu})}{\epsilon_{\rm TOT} \int Ldt}$$

where $N_{\rm cand}$ is the number of candidate events, $f_{\rm bb}$, f_{cosmic}, $f_{\tau\tau}$ and $f_{W\rightarrow\mu\nu}$ are the fraction of the candidate events attributed to $b\bar{b}$, cosmic rays, $Z \rightarrow \tau^+\tau^-$ and $W \rightarrow \mu\nu$ respectively, $\int Ldt$ is the integrated luminosity of the data sample [1] and $\epsilon_{\rm TOT}$ is the efficiency of the selection cuts. The acceptance is evaluated using a parameterised simulation of the DØ detector with the tracking, muon identification and trigger efficiencies introduced from measurements made on data. The data sample is split into three separate periods due to variation in tracking, muon identification and trigger efficiencies. During the first data taking period (period 1, 36 pb^{-1}), containing all runs before run 173482, only the di-muon trigger was unprescaled. After this run data was taken using both the di-muon and single muon triggers (period 3, 109 pb^{-1}). 1.5 pb^{-1} of data collected over the same time period but using only the di-muon trigger as the single muon trigger was prescaled are also treated separately. Periods 1 and 2 are distinguished to reflect the increased tracking, muon identification and trigger efficiencies in later runs. $\sigma(p\bar{p} \rightarrow Z/\gamma \rightarrow \mu^+\mu^-)$ is evaluated separately for each of these periods which are combined only for the final measurement.

A measurement of the cross section for pure Z boson exchange, $p\bar{p} \rightarrow Z \rightarrow \mu^+\mu^-$, is obtained by correcting the cross section for all pure γ^* and Z/γ interference terms so that only the pure Z propagator is considered. The ratio of the $Z \rightarrow \mu^+\mu^-$ to $W \rightarrow \mu\nu$ cross sections can be used to derive an indirect measurement of the total width of the W boson, which can be used to test the standard model. The $Z \rightarrow \mu^+\mu^-$ cross section can also be used in the search for physics beyond the standard model.

This note only gives a brief overview of this analysis. Interested readers are directed to reference [2] for a detailed description.

II. THE DØ DETECTOR

The Run II DØ detector consists of the following main elements [3, 4]. A central-tracking system, consisting of a silicon microstrip tracker (SMT) and a central fiber tracker (CFT), both located within a 2 T superconducting solenoidal magnet. The SMT was designed to optimize tracking and vertexing within $|\eta| < 3$. The system has a six-barrel longitudinal structure interspersed with 16 radial disks. The CFT has eight thin coaxial barrels, each supporting two doublets of overlapping scintillating fibers of 0.835 mm diameter, one doublet being parallel to the collision axis, and the other alternating by $\pm 3^\circ$ relative to the axis. Light signals are transferred via clear light fibers to solid-state photon counters (VLPC) that have $\approx 80\%$ quantum efficiency.

Central and forward preshower detectors located just outside of the magnet are constructed of several layers of scintillator strips. The next layer of detection involves three liquid-argon/uranium calorimeters: a central section (CC) covering $|\eta|$ up to ≈ 1, and two end calorimeters (EC) extending coverage to $|\eta| \approx 4$.

A muon system resides beyond the calorimetry, and consists of a layer of tracking detectors and scintillation trigger counters before 1.8 T toroids, followed by two more similar layers after the toroids. Tracking at $|\eta| < 1$ relies on 10 cm wide drift tubes, while 1 cm mini-drift tubes are used at $1 < |\eta| < 2$. Coverage for muons is partially compromised in the region of $4.25 < \phi < 5.15$ for $|\eta| < 1.25$, where the calorimeter is supported mechanically from the ground. For mechanical reasons each layer of scintillators and trackers is divided into eight regions, or 'octants', in ϕ separated by small gaps.

Luminosity is measured using plastic scintillator arrays located in front of the EC cryostats, covering $2.7 < |\eta| < 4.4$. The trigger and data acquisition systems are designed to accommodate the large luminosity of Run II. Based on preliminary information from tracking, calorimetry, and muon systems, the output of the first level of the trigger is used to limit the rate for accepted events to ≈ 1.5 kHz. At the next trigger stage, with more refined information, the rate is reduced further to ≈ 800 Hz. These first two levels of triggering rely purely on hardware and firmware. The third and final level of the trigger, with access to all the event information, uses software algorithms and a computing farm, and reduces the output rate to ≈ 50 Hz, which is written to tape.

III. EVENT SELECTION CUTS: $Z \to \mu^+\mu^-$ SIGNAL SAMPLE

The event selection requires evidence that a pair of oppositely charged muons with high momentum in the direction transverse to the beam pipe, p_T, are produced. Muons are identified by requiring a track in the muon system matched to a track in the central tracking system. The p_T of the muon is determined solely using the information from the central tracking system. The muon identification criteria require that the track in the muon system has scintillator and wire hits associated with it either in the layer inside or outside the toroid volume.

The muons are required to lie within the nominal geometrical acceptance of the muon chambers. This excludes the region where $|x| < 110$ cm and $|y| < 110$ cm, where x and y are the co-ordinates of a muon as it enters the muon system. The compromised region of the muon system containing the calorimeter supports, defined by $4.25 < \phi < 5.15$ for $|\eta| < 1.25$, is also excluded. Unless otherwise stated the pseudo-rapidity η is measured at the position that the muons enter the muon system.

The following additional selection criteria are applied:

1. $p_T > 15$ GeV for both muons.
2. $M_{\mu\mu} > 40$ GeV, where $M_{\mu\mu}$ is the invariant mass of the di-muon pair.
3. To reduce the background from $b\bar{b}$ events where both b quarks decay semi-leptonically into muons, at least two out of the following four isolation criteria should be satisfied.
   (a) $\Sigma_{\rm tracks,i}({p_T}^i) < 3.5$ GeV, where $\Sigma_{\rm tracks,i}({p_T}^i)$ is the sum of the p_T of tracks contained within a cone around the first muon direction with opening angle $R < 0.5$, where $R^2 = \Delta\eta^2 + \Delta\phi^2$.
   (b) Same as (a) but for the second muon.
   (c) $\Sigma_{\rm cells,i}(E_T^i) < 2.5$ GeV, where $\Sigma_{\rm cells,i}(E_T^i)$ is the sum of the transverse energies of calorimeter cells for $0.1 < R < 0.4$ around the direction of the first muon.
   (d) Same as (c) but for second muon.
4. To reduce the background from cosmic ray muons traversing the detector:
   (a) $dca < 0.02$ cm for muon tracks containing SMT hits and $dca < 0.2$ cm for muon tracks with no SMT hits, where dca is the distance of closest approach to the beam spot position in the $r\phi$ plane.
   (b) Events in which the muons are exactly back to back are removed by requiring $\Delta\alpha_{\mu\mu}$ to be > 0.05 radians, where $\Delta\alpha_{\mu\mu} = |\Delta\phi_{\mu\mu} + \Delta\theta_{\mu\mu} - 2\pi|$.
5. In data taking periods 1 and 2 events could only be selected if they passed the di-muon trigger [12]. In data taking period 3 events could be selected if they passed either the di-muon or the single muon trigger.

   For an event to pass the di-muon trigger both muons must have hits in the scintillation counters identified by the first Level of the trigger system (The 'L1 scint' requirement). At the second Level of the trigger the hits in the muon system are combined in a basic fit. The di-muon trigger requires that at least one of the muons has a track reconstructed in the muon system (The 'L2M0' requirement). Before run 173482 the di-muon trigger only fired if there were hits in both luminosity detectors (the fast-z requirement).

   For an event to pass the single muon trigger either muon must have hits in both the scintillation counters and the drift chambers identified by the first Level of the trigger system (The 'L1 wire' requirement). These hits must be in the region $|\eta| < 1.5$. The single muon trigger requires that at least one of the muons has a track reconstructed in the muon system, at the second Level of the trigger, with a $p_T > 3$ GeV (The 'L2M3' requirement). The single muon trigger requires that at least one of the muons has a track reconstructed by the third Level of the trigger system with a $p_T > 10$ GeV (The 'L3TK' requirement).

The total number of candidate events after this selection is 14352.

IV. BACKGROUNDS

There have been four backgrounds identified as contributing to the candidate events: $b\bar{b}$, cosmic rays, $Z \to \tau^+\tau^-$ and $W \to \mu\nu$.

The background fraction due to $b\bar{b}$, $f_{\rm bb}$, is evaluated from data using the fact that muons produced in $b\bar{b}$ events are produced in association with other particles so tend not to be isolated. The level of the remaining $b\bar{b}$ background can be estimated by considering the number of like sign charge di-muon events that satisfy all other selection criteria but

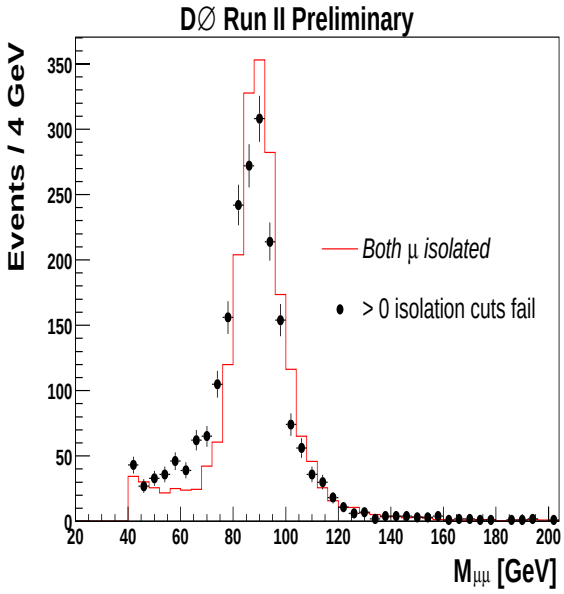

FIG. 1: Distribution of $M_{\mu\mu}$ for events where at least one of the isolation cuts fails (points with error bars) and for events where all isolation cuts pass (histogram).

are not perfectly isolated. After taking into account the efficiency of the opposite sign charge requirement and the ratio of like sign charge to unlike sign charge $b\bar{b}$ events $f_{\rm bb}$ is evaluated to be 0.005 ± 0.003.

As a cross-check that this estimate is reasonable the distribution of $M_{\mu\mu}$ for candidate events where all of the four isolation criteria pass and that of candidate events where at least one of the isolation criterion fails is plotted in Figure 1. The two distributions are normalised to the same number of events in the region $M_{\mu\mu} > 50$ GeV. The di-muon mass peak appears to be wider and shifted towards lower masses if one of the muons is non-isolated, as would be expected in events with final state bremsstrahlung. In these events the photon causes the muon to be non-isolated. Apart from this feature the two distributions have similar shapes indicating that the level of $b\bar{b}$ background is small.

The residual cosmic ray background contamination f_{cosmic} is measured from data using the distribution of the time difference between the two muons, measured with the muon detector scintillators, as a function of $\Delta\alpha_{\mu\mu}$: $f_{cosmic} = 0.001 \pm 0.001$.

Events where a Z boson is produced which subsequently decays to two τs which themselves both decay to two muons are difficult to distinguish from $Z \to \mu^+\mu^-$ events. The fraction of candidate events attributable to $Z \to \tau^+\tau^-$ is evaluated using PYTHIA Monte Carlo passed through a GEANT [5] based simulation of the DØ detector. This is used instead of the parameterised simulation due to the difficulty of modelling events where the hadronic decays of the τ fake a muon. Samples of $Z \to \mu^+\mu^-$ and $Z \to \tau^+\tau^-$ are generated and the ratio of the number of events selected in the two samples is used to determine the fraction of candidate events attributable to $Z \to \tau^+\tau^-$. Following this procedure the background fraction due to $Z \to \tau^+\tau^-$ is determined to be $f_{\tau\tau} = 0.005 \pm 0.001$.

A $W \to \mu\nu$ event may represent a background to the muon pair sample if it contains an additional high p_T muon. The probability for this to occur is estimated by measuring the fraction of candidate events where there is more than one pair of muons that pass the selection cuts described above, since the fraction of $Z \to \mu^+\mu^-$ events containing an additional muon is assumed to be the same as that for $W \to \mu\nu$ events. After allowing for the larger $W \to \mu\nu$ cross section, this background is determined to be $f_{W\to\mu\nu} = 0.002 \pm 0.001$.

V. MEASUREMENT OF TRACKING, MUON IDENTIFICATION AND TRIGGER EFFICIENCIES

The tracking, muon identification and trigger efficiencies are measured from data using the 'tag and probe' method. This utilises the ability to select a clean sample of $Z \to \mu^+\mu^-$ events even if one of the muons has no track associated with it or is not identified in the muon system and fails to meet the trigger requirements.

An event is tagged as a $Z \to \mu^+\mu^-$ event if it contains a 'tag' muon with tight requirements in both the central and muon detectors and a 'probe' muon, identified using all requirements other than that being probed. The efficiency is

the fraction of events in which the probe requirement is met. If both muons satisfy the requirements of the 'tag' and 'probe' muons the event is used twice in the efficiency calculation.

In the following sections approximate average values are given for the tracking, muon identification and trigger efficiencies. However, in order to properly account for geometrical correlations between these different efficiencies they are measured as a function of position in the detector. These position-dependent efficiencies are simulated in the Monte Carlo used to evaluate the overall detection efficiency.

A. Tracking Efficiency

The 'tag' muon is selected with a track associated with it in both the tracking detectors with $p_T > 30$ GeV and in the muon system. The 'probe' muon is identified by a track in the muon system, with $p_T^{\rm local} > 15$ GeV, where $p_T^{\rm local}$ is the momentum measured in the muon chambers. If there is a central track associated with the 'probe' muon the event is counted as 'efficient', otherwise it is counted as 'inefficient'.

Figure 2 shows a schematic view of the event selection for this control sample.

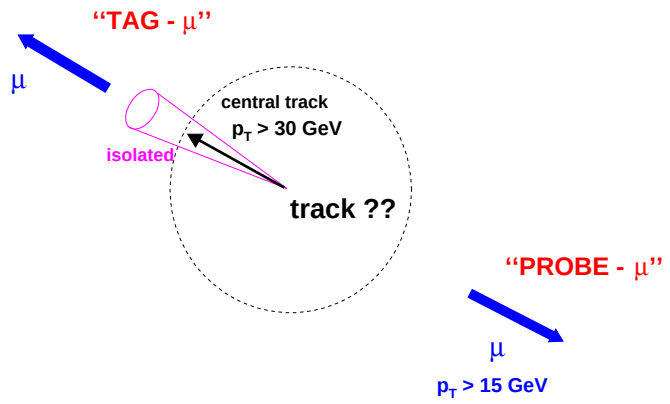

FIG. 2: Schematic view of the event selection for tracking efficiency sample.

In order to demonstrate that the level of background in the 'efficient' and 'inefficient' samples is similar the left hand plot in Figure 3 shows the p_T of the control muon for events where the test muon is found to have a central track associated with it on top of that for events where the test muon is found not to have a central track associated with it. The distributions are normalised to the same number of events. The slight discrepancy in the two distributions is due to the η distribution of the different samples. The tracking efficiency falls off at high η where the average p_T of the muons is smaller. From the numbers of test muons in the 'efficient' and 'inefficient' subsamples an average value for the tracking efficiency of

$$\epsilon_{\rm track} = 0.951 \pm 0.002$$

is found. The tracking efficiency is introduced into the Monte Carlo as a function of CFT detector η in bins of the z position of the muon track. The right hand plot in Figure 3 shows the tracking efficiency as a function of CFT detector η for $|z| < 10$ cm.

B. Muon Identification Efficiency

The 'tag' muon is selected with a track associated with it in both the tracking detectors with $p_T > 30$ GeV and in the muon system. The muon identification criteria used for the 'tag' muon are made more stringent, requiring hits in scintillators and tracking detectors associated with the muon track in layers both inside and outside the toroid. The control muon is required to satisfy the requirements of a single muon trigger that ensured the event was written to tape.

The test muon is identified by requiring a track in the central detector of $p_T > 20$ GeV. If there is a muon, satisfying the identification criteria used in this analysis, associated with the 'probe' track the event is counted as 'efficient'. If there is no such track the event is counted as 'inefficient'.

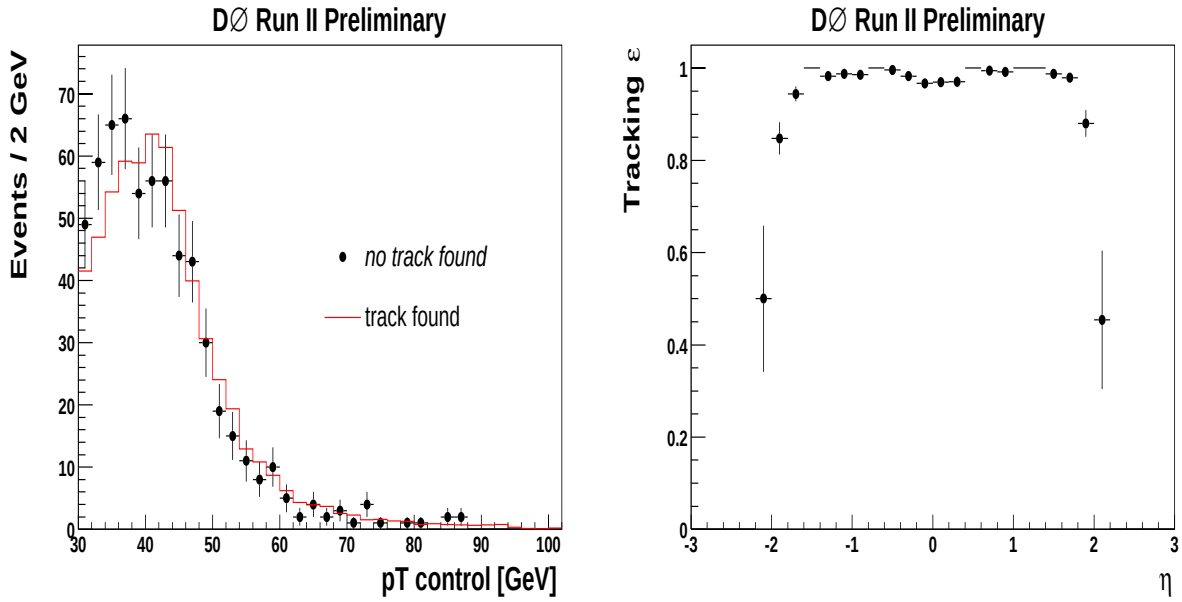

FIG. 3: **Tracking efficiency study:** Left hand plot: p_T of the control muon. Solid histogram: Events where the test muon is matched to a central track. Points with errors: Events where the test muon is not matched to a central track. Right hand plot: The tracking efficiency as a function of CFT detector η for $|z| < 10$ cm, where z is the z-position of the muon track.

Figure 4 shows a schematic view of the event selection for this control sample.

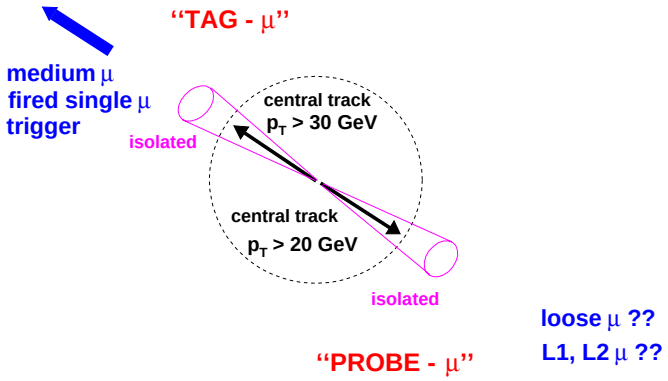

FIG. 4: Schematic view of the event selection for muon identification and trigger efficiency sample.

In order to demonstrate that the level of background in the 'efficient' and 'inefficient' samples is similar Figure 5 shows the distribution of $M_{\mu\mu}$ for events where the test track is found to have a muon associated with it on top of that for events where the test muon is found not to have a muon associated with it. The distributions are normalised to the same number of events.

The efficiency of the muon identification criteria in the regions close to the boundaries between the octants of the muon chambers is significantly lower than for the rest of the azimuthal angle as shown in Figure 6 (left hand plot). This dependency of the efficiency on ϕ is taken into account in the calculation of the acceptance as discussed in section VI A.

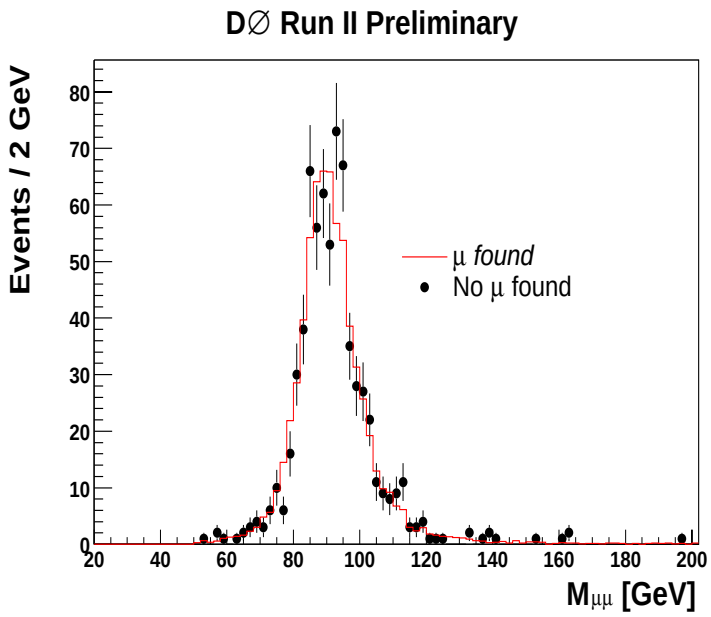

FIG. 5: $M_{\mu\mu}$ for the muon identification efficiency study. Histogram shows those events where a muon is identified. Points with error bars shows those events where no muon is identified.

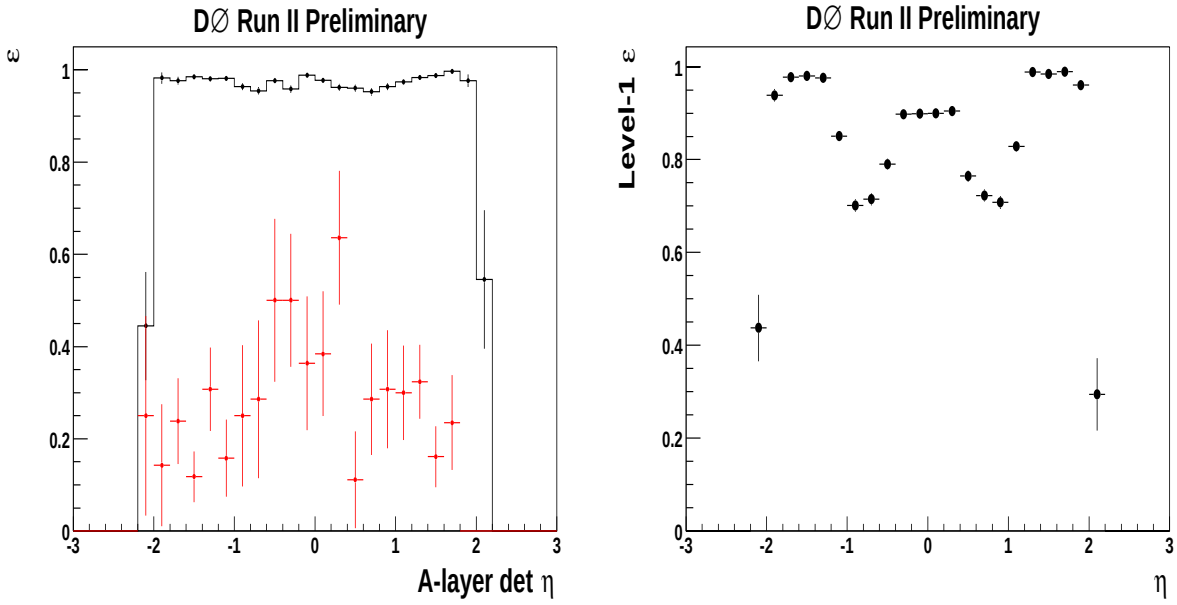

FIG. 6: Left hand plot: The muon identification efficiency as a function of η in the boundary regions (lower points) and outside the boundary region (higher points). Right hand plot: The 'L1 scint' efficiency as a function of muon detector η with respect to a reconstructed muon.

C. Trigger Efficiencies

For the measurement of the trigger efficiencies events are used which pass all the selection cuts except different trigger requirements are made.

To evaluate the 'L1 scint', 'L1 wire', 'L2M0' and 'L2M3' conditions the control muon is required to fire the single muon trigger and the fraction of events in which the condition in question is met for the probe muon is the efficiency. The efficiency of the 'L1 scint' requirement is shown as a function of η in the right hand plot in Figure 6. To evaluate

Efficiency of	measured with respect to	ε
Muon Identification (M)		0.939 ± 0.002
'L1 scint'(L1S)	M	0.858 ± 0.002
'L1 wire' (L1W)	M and LS	0.749 ± 0.003
'L2M0'[a]	M and L1S	0.931 ± 0.002
'L2M3'	M and L1S and L1W	0.971 ± 0.001
'L3TK'	track	0.789 ± 0.003

[a]The efficiency quoted here is for the latter two data taking periods. The Level-2 efficiency increased at a certain stage with the dataset used and therefore the efficiency is measured separately for the 2 periods

TABLE I: Muon identification and trigger average efficiencies.

the 'L3TK' condition efficiency the event is required to fire the di-muon trigger.

An approximation to the average value of all the muon chamber trigger and reconstruction efficiencies is shown in Table I.

VI. DETERMINATION OF CROSS SECTIONS

A. Evaluation of Efficiencies

The total acceptance for $p\bar{p} \to Z/\gamma \to \mu^+\mu^-$, including trigger and selection efficiencies and geometrical acceptance, $\epsilon_{\rm TOT}$, is evaluated, in each data taking period, according the following formula:

$$\epsilon_{\rm TOT} = \epsilon^{\rm eff}_{\rm MC} \times \epsilon_{\rm fz} \times \epsilon_{\rm opposite\_q} \times \epsilon_{\rm isol} \times \epsilon_{\rm cosmic}$$

where the symbols are defined as follows;

1. $\epsilon^{\rm eff}_{\rm MC}$ takes into account the geometrical acceptance of the muon chambers and the efficiency of the 'kinematic' cuts on p_T and $M_{\mu\mu}$. It also includes the trigger, tracking and muon identification efficiencies. $\epsilon^{\rm eff}_{\rm MC}$ is evaluated separately for the three data taking periods. Further details are described below.

2. $\epsilon_{\rm fz}$ is the efficiency for the fast z trigger requirement. This was determined using $Z \to e^+e^-$ data selected using triggers independent of this requirement and examining the fraction of events in which the the fast-z trigger fired, $\epsilon_{\rm fz} = 0.943 \pm 0.005$. This requirement was omitted after the first data taking period and so in periods 2 and 3 $\epsilon_{\rm fz}$ is trivially 1.

3. $\epsilon_{\rm opposite\_q}$ is the efficiency for the cut requiring that the muons have opposite sign charges. To estimate $\epsilon_{\rm opposite\_q}$, the ratio of like-sign to unlike-sign events is studied for different quality requirements on the tracks. The efficiency for the opposite charge requirement is $\epsilon_{\rm opposite\_q} = 0.998 \pm 0.001$.

4. $\epsilon_{\rm isol}$ is the efficiency for the cut requiring that an event is isolated. The value of $\epsilon_{\rm isol}$ is estimated by fitting a $Z \to \mu^+\mu^-$ peak to those events failing the isolation cuts. $\epsilon_{\rm isol} = 0.996 \pm 0.002$.

5. $\epsilon_{\rm cosmic}$ is the efficiency for the event to pass the cuts designed to eliminate cosmic rays. By studying the $M_{\mu\mu}$ distribution and timing information for events rejected by the cuts on $\Delta\alpha_{\mu\mu}$ and dca, and cross-checking using the Monte Carlo, the efficiency of these cuts is concluded to be $\epsilon_{\rm cosmic} = 0.988 \pm 0.006$.

Apart from $\epsilon_{\rm fz}$ and $\epsilon^{\rm eff}_{\rm MC}$ all efficiencies are assumed to be constant across the three data taking periods.

$\epsilon^{\rm eff}_{\rm MC}$ takes into account the geometrical acceptance of the muon chambers and the efficiency of the 'kinematic' cuts on p_T and $M_{\mu\mu}$. It also includes the trigger, tracking and muon identification efficiencies. It is determined using a parameterised simulation of the DØ detector and the PYTHIA generator [6] employing the CTEQ6M PDF set [7]. To evaluate $\epsilon^{\rm eff}_{\rm MC}$ a sample of $p\bar{p} \to Z/\gamma \to \mu^+\mu^-$ is generated with a generator level mass cut of 30 GeV. This lower mass cut is to account for those events with a physical invariant mass less than 40 GeV, but which are measured to have a mass greater than 40 GeV and so are included within the acceptance. $\epsilon^{\rm eff}_{\rm MC}$ is defined to be the ratio between the number of events accepted to the number of events generated with a mass greater than 40 GeV.

The tracking, muon identification and trigger efficiencies are measured in data, as described in section V. Each efficiency is then introduced in the Monte Carlo by accepting a condition (eg has track, identified as muon, etc)

Period	$\epsilon_{\rm MC}^{\rm eff}$	$\sigma_{\epsilon_{\rm MC}^{\rm eff}}$ (Stat)	$\sigma_{\epsilon_{\rm MC}^{\rm eff}}$ (Syst)	integrated luminosity, $\int Ldt$
One	0.239	0.006	0.004	36.8
Two	0.268	0.002	0.004	1.5
Three	0.322	0.002	0.004	109.4

TABLE II: Variation of $\epsilon_{\rm MC}^{\rm eff}$ associated uncertainties in the three time periods.

with probability $P(\eta, \phi)$. A check to ensure that the efficiencies are unbiased is performed using a GEANT based simulation comparing the efficiencies obtained by the tag and probe method with those obtained using the Monte Carlo truth information.

Events are selected if they pass the event selection as described in section III.

Table II lists the value of $\epsilon_{\rm MC}^{\rm eff}$ with its associated uncertainty for the three periods. The evaluation of uncertainties is described below. The increase in $\epsilon_{\rm MC}^{\rm eff}$ in the second period, with respect to the first, is due to increased tracking, muon identification and trigger efficiencies. The increase in $\epsilon_{\rm MC}^{\rm eff}$ in the third period, with respect to the second, is entirely due to the use of the single muon trigger.

The uncertainty on $\epsilon_{\rm MC}^{\rm eff}$ due to Monte Carlo statistics is negligible as 2 million events were used. The statistical uncertainty, as quoted in table II, arises from the statistical uncertainty on the input efficiencies as measured in the data. The accuracy with which these efficiencies are known is determined from the data and the uncertainty is evaluated by varying each of the efficiencies when they are introduced into the simulation. Simultaneously the value of the efficiency in each bin is varied independently with a Gaussian distribution with sigma equal to the size of the uncertainty on that bin. This is done 100 times and the statistical uncertainty is given by the standard deviation of the $\epsilon_{\rm MC}^{\rm eff}$ values obtained.

There is also some uncertainty from small imperfections in the way the the detector is modelled by the Monte Carlo. The largest factor arises from the uncertainty in how the octant boundaries are defined in the muon identification efficiency. The boundary region is varied, the change in acceptance examined and a 1.0% uncertainty on $\epsilon_{\rm MC}^{\rm eff}$ quoted. Uncertainty on the distribution of the beampsot in the z-direction leads to a 0.6% uncertainty on $\epsilon_{\rm MC}^{\rm eff}$. There is an uncertainty of 0.5% caused by an assesment of the background content in the 'L1 scint' efficiency, 0.5% uncertainty caused by averaging the efficiencies within the different run periods. An uncertainty of 0.5% is attributed to normalising 1D projections in the 'L1 scint' efficiency, p_T resolution and scale and backgrounds in the tracking efficiency study.

The effect on $\epsilon_{\rm MC}^{\rm eff}$ of varying the choice of PDF was investigated using the method suggested by the CTEQ collaboration and the associated PDF sets [7]. The uncertainty in $\epsilon_{\rm MC}^{\rm eff}$ due to the choice of PDF is found to be 1.7% using this method.

B. Extraction of $p\bar{p} \rightarrow Z \rightarrow \mu^+\mu^-$ Cross Section Using the Drell-Yan Correction

The acceptance quoted is that for the physical process $Z/\gamma \rightarrow \mu^+\mu^-$. In order to extract the cross section for $p\bar{p} \rightarrow Z \rightarrow \mu^+\mu^-$, the contributions to the candidate event sample expected from photon exchange and Z/γ interference are 'corrected for' by applying a factor:

$$R_\sigma = \sigma_Z/\sigma_{TOT},$$

where R_σ is the ratio between the non-physical cross section solely due to pure Z exchange (σ_Z) and that for full Z/γ exchange (σ_{TOT}). These cross sections are evaluated using the NLO Monte Carlo program, MC@NLO[9]. σ_{TOT} is the cross section for a propagator mass greater than or equal to 40 GeV.

The value of R_σ has a systematic uncertainty due to the choice of PDF. This uncertainty has some correlation with the PDF uncertainty on $\epsilon_{\rm MC}^{\rm eff}$. To account for this correlation the PDF uncertainty in the $\sigma \times$ Br for pure Z exchange is for the ratio of R_σ and $\epsilon_{\rm MC}^{\rm eff}$. Following this method the PDF uncertainty is found to be 1.7%. In the table III this uncertainty is associated with R_σ to avoid any arbitrary splitting between quantities.

C. Determination of Results

The cross section for the process $p\bar{p} \rightarrow Z/\gamma \rightarrow \mu^+\mu^-$ is evaluated according to the following formula:

$$\sigma(p\bar{p} \rightarrow Z/\gamma \rightarrow \mu^+\mu^-) = \frac{N_{\rm cand}(1 - f_{\rm bb} - f_{cosmic})(1 - f_{\tau\tau})(1 - f_{W\rightarrow\mu\nu})}{\epsilon_{\rm TOT} \int Ldt}$$

Table III summarises the various contributions to the cross section and its uncertainty that remain constant throughout the entire dataset.

Quantity	Value	Uncertainty	Contribution to fractional uncertainty on $\sigma \times$ Br
opposite charge, $\epsilon_{\text{opposite\_q}}$	0.998	0.001	0.001
muon isolation, ϵ_{isol}	0.996	0.002	0.002
cosmic veto, ϵ_{cosmic}	0.988	0.006	0.006
$b\bar{b}$ backgrounds, f_{bb}	0.005	0.003	0.003
$\text{Z} \to \tau^+\tau^-$ backgrounds, $f_{\tau\tau}$	0.005	0.001	0.001
Cosmic backgrounds, f_{cosmic}	0.001	0.001	0.000
$\text{W} \to \mu\nu$ backgrounds, $f_{\text{W}\to\mu\nu}$	0.002	0.001	0.000
Drell-Yan correction, R_σ	0.885	0.015	0.017

TABLE III: *Summary of the components to the calculation of the cross section and the various contributions to the cross section times branching ratio uncertainty that remain constant throughout the data taking period.*

Tables IV – VI summarise the calculation of the various contributions to the cross section and its uncertainty for the three data taking periods. The uncertainty on $\epsilon_{\text{MC}}^{\text{eff}}$ is due to the uncertainty on the input efficiencies.

The final cross section for the process $\text{p}\bar{\text{p}} \to \text{Z}/\gamma \to \mu^+\mu^-$ is obtained:

$$\sigma(\text{p}\bar{\text{p}} \to \text{Z}/\gamma \to \mu^+\mu^-) = 329.2 \pm 3.4(\text{stat.}) \pm 7.8(\text{syst.}) \pm 21.4(\text{lumi.}) \ \text{pb}.$$

Correcting the number of di-muon events by a factor of $R_\sigma = 0.885 \pm 0.015$ for the contribution from pure photon exchange and Z/γ interference, the result

$$\sigma(\text{p}\bar{\text{p}} \to \text{Z} \to \mu^+\mu^-) = 291.3 \pm 3.0(\text{stat.}) \pm 6.9(\text{syst.}) \pm 18.9(\text{lumi.}) \ \text{pb}$$

is obtained.

Figure 7 shows the theoretical prediction [10] of $\sigma \times$ Br for $\text{p}\bar{\text{p}} \to \text{Z} \to ll$ as a function of centre of mass energy with the measurements made by DØ and CDF [11] in the electron, muon and tau channels.

Quantity	Value	Uncertainty	Contribution to fractional uncertainty on $\sigma \times$ Br
integrated luminosity, $\int Ldt(\mathrm{pb}^{-1})$	36.8	2.392	0.065
number of candidates, $\mathrm{N_{cand}}$	2650	51.5	0.019
Monte Carlo with efficiencies, $\epsilon_{\mathrm{MC}}^{\mathrm{eff}}$	0.239	0.006	0.025
_fz trigger, ϵ_{fz}	0.943	0.004	0.004
$\sigma \times$ Br (pb)	284.2	9.1	0.032

TABLE IV: *Summary of the components to the calculation of* $\sigma \times$ Br *and the contributions to the* $\sigma \times$ Br *uncertainty for the first run period.*

Quantity	Value	Uncertainty	Contribution to fractional uncertainty on $\sigma \times$ Br
integrated luminosity, $\int Ldt(\mathrm{pb}^{-1})$	2.5	0.0975	0.065
number of candidates, $\mathrm{N_{cand}}$	146	12.1	0.083
Monte Carlo with efficiencies, $\epsilon_{\mathrm{MC}}^{\mathrm{eff}}$	0.268	0.002	0.009
_fz trigger, ϵ_{fz}	1	0	0.000
$\sigma \times$ Br (pb)	323.0	26.9	0.083

TABLE V: *Summary of the components to the calculation of* $\sigma \times$ Br *and the contributions to the* $\sigma \times$ Br *uncertainty for the second run period.*

Quantity	Value	Uncertainty	Contribution to fractional uncertainty on $\sigma \times$ Br
integrated luminosity, $\int Ldt(\mathrm{pb}^{-1})$	109.4	7.111	0.065
number of candidates, $\mathrm{N_{cand}}$	11556	107.5	0.009
Monte Carlo with efficiencies, $\epsilon_{\mathrm{MC}}^{\mathrm{eff}}$	0.322	0.002	0.006
_fz trigger, ϵ_{fz}	1	0	0.000
$\sigma \times$ Br (pb)	291.8	3.2	0.011

TABLE VI: *Summary of the components to the calculation of* $\sigma \times$ Br *and the contributions to the* $\sigma \times$ Br *uncertainty for the third run period.*

D. Data - Monte Carlo Comparison Plots and Cross Checks

In order to demonstrate that the Monte Carlo simulation provides a realistic description of the data a series of comparison plots are included and a series of cross checks performed listed. In each of the comparison plots the data is shown as points with error bars, the Monte Carlo is shown as a solid histogram and the uncertainty on the Monte Carlo is shown as shaded bands. In each plot the Monte Carlo has been normalised to the number of events in data.

Figure 8 compares the mass distribution of the total sample in data and Monte Carlo. The $\mathrm{Z} \rightarrow \tau^+\tau^-$ and $b\bar{b}$ background are also shown.

Figures 9 and 10 show the distribution of η and ϕ respectively for the candidate muons in the first and third data taking periods.

Figure 11 shows the p_T distribution of the Z boson for the candidate data events in the whole data taking period. The plot is displayed in two forms: the left hand plot shows the low p_T region alone and the right hand plot shows a more extended range with the aid of a logarithmic scale.

A series of cross checks is listed here:

1. The geometrical and kinematic efficiencies have been evaluated using the HERWIG Monte Carlo program[8] and there is good agreement between the acceptances in HERWIG (0.406 ± 0.001), and PYTHIA (0.405 ± 0.002).

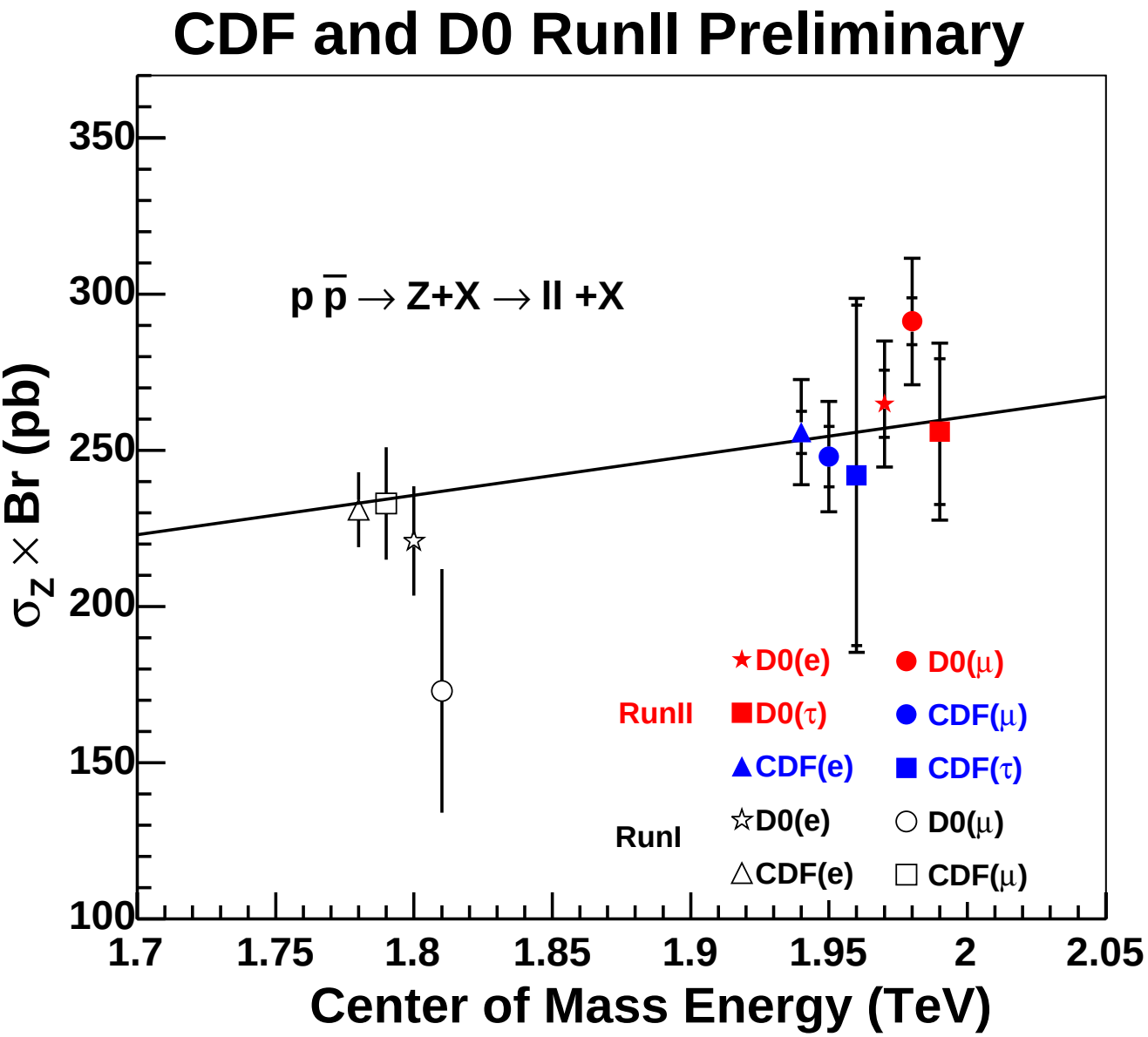

FIG. 7: The theoretical prediction of $\sigma \times \mathrm{Br}$ for $\mathrm{p\bar{p}} \to \mathrm{Z} \to ll$ as a function of the centre of mass energy as predicted in [10]. The experimental measurements in the muon and electron channels for the DØ and CDF [11] experiments are shown as points with error bars.

2. The mass cut is moved to 30, 50 and 60 GeV and the $\mathrm{Z} \to \mu^+\mu^-$ cross section increases by 0.2%, 0.3% and 0.6% respectively.

3. The trigger efficiency is evaluated using events selected by calorimeter based triggers. The single muon trigger in the third period is found to be 0.86 ± 0.01 compared with the value of 0.846 found by measuring component efficiencies.

4. The cross section, in the last period, is evaluated for the di-muon and single muon triggers separately and found to be 287.6 and 292.0 respectively, where the uncorrelated uncertainty on the difference between these figures is 1.0%.

5. The cross section is evaluated for events where both muons are in the central region ($|\eta| < 1$) to be $289.8 \pm 4.3\mathrm{pb}^{-1}$, where both muons are not in the central region to be $287.5 \pm 7.5\mathrm{pb}^{-1}$ and where one muon is and the

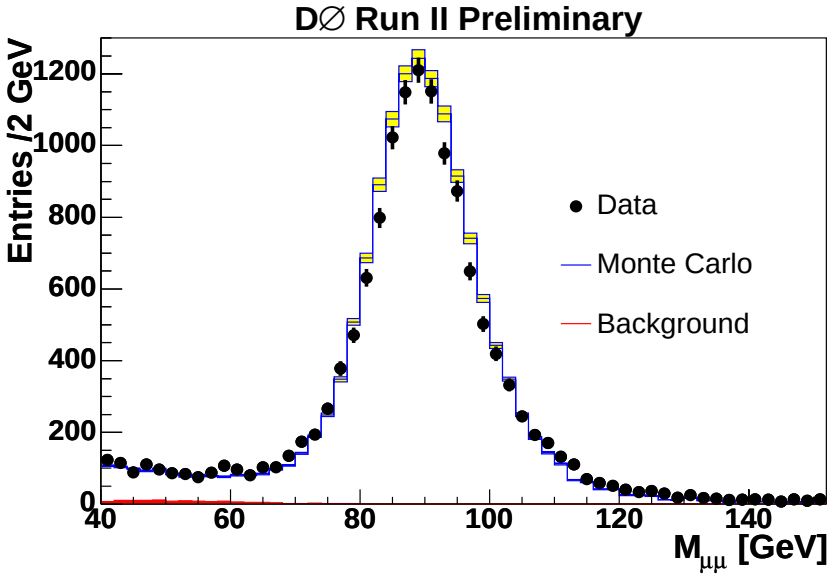

FIG. 8: Comparison of $M_{\mu\mu}$ for candidate events with Monte Carlo prediction. The data are shown as points with error bars. The prediction of Monte Carlo is shown as the open histogram. The contribution from the background is shown as the shaded filled histogram.

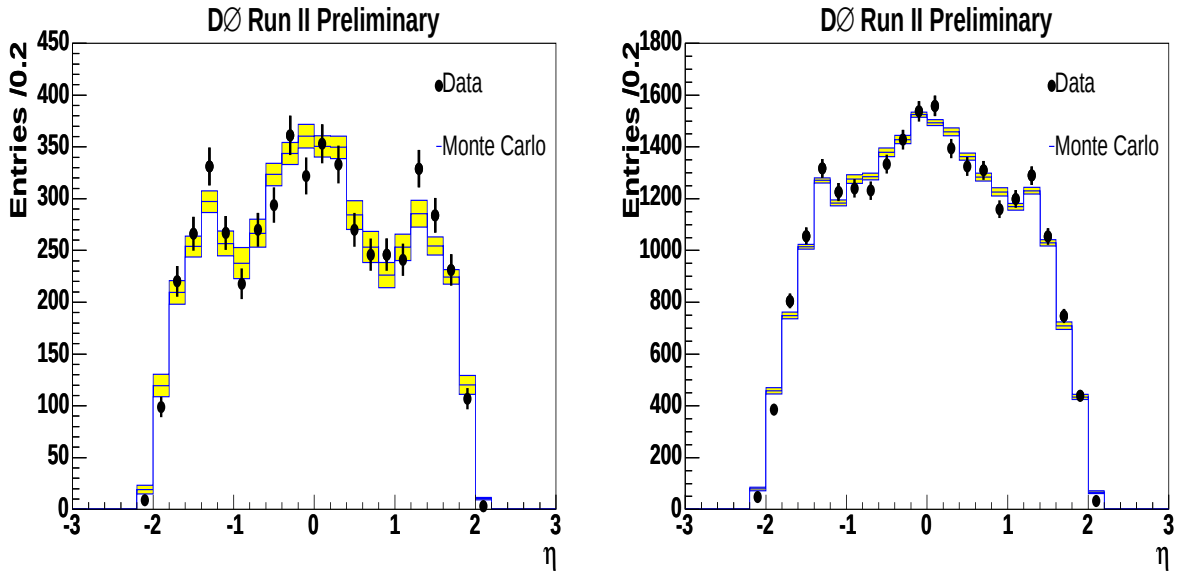

FIG. 9: Comparison of η distribution of candidate muons with Monte Carlo prediction. The data are shown as points with error bars. The prediction of smeared Monte Carlo is shown as the open histogram. Left hand plot: Period 1. Right hand plot: Period 3.

other is not to be $293.6 \pm 4.1 \text{pb}^{-1}$. The uncertainties on these cross sections are solely due to the number of candidate events.

6. The isolation criteria in the efficiency samples differ slightly from those in the candidate events. The efficiency is determined separately for isolated and non-isolated events and then weighted to reflect the fraction of isolated and non isolated events in the data. This had a negligible effect of the total cross section.

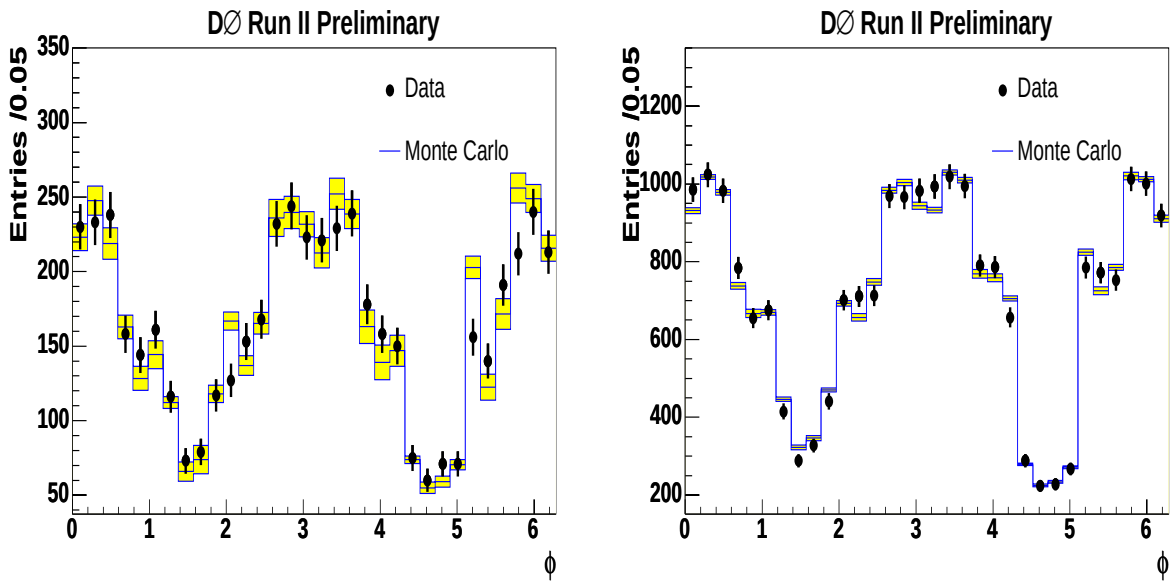

FIG. 10: Comparison of ϕ distribution of candidate muons with Monte Carlo prediction. The data are shown as points with error bars. The prediction of Monte Carlo is shown as the open histogram. Left hand plot: Period 1. Right hand plot: Period 3.

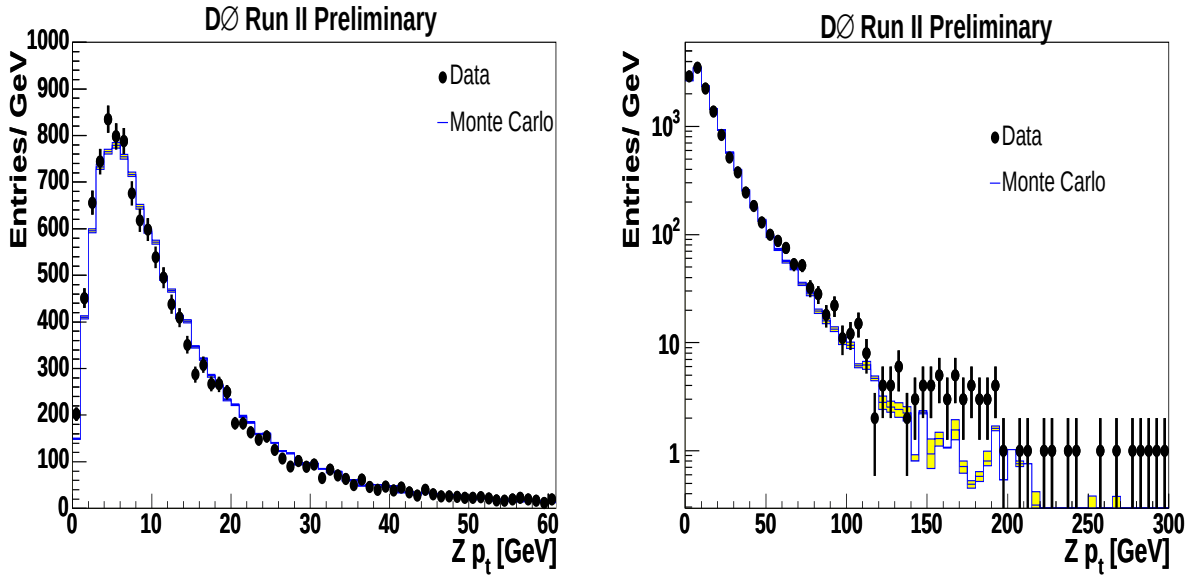

FIG. 11: Comparison of p_T distribution of Z boson with Monte Carlo prediction. The data are shown as points with error bars. The prediction of Monte Carlo is shown as the open histogram (Periods 1 and 3). Left hand plot: Low p_T region. Right hand plot: Entire p_T range (log scale).

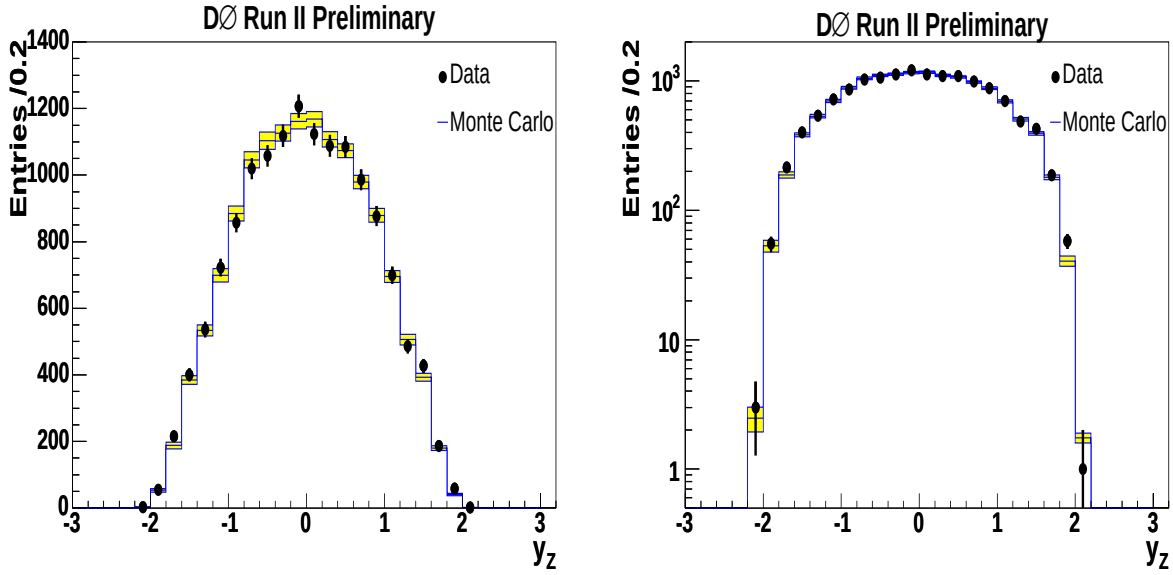

FIG. 12: Comparison of the rapdity distribution of the Z boson with Monte Carlo prediction. The data are shown as points with error bars. The prediction of Monte Carlo is shown as the open histogram (Periods 1 and 3). Left hand plot: linear scale. Right hand plot: log scale.

[1] T. Edwards *et al.*, DØ Note **4328** (2003)
[2] E. Nurse and P. Telford, DØ Note **XXXX** (2004)
[3] S. Abachi, *et al.*, Nucl. Instrum. Methods Phys. Res. A **338**, 185 (1994).
[4] V. Abazov, *et al*, in preparation for submission to Nucl. Instrum. Methods Phys. Res. A, and T. LeCompte and H.T. Diehl, "The CDF and DØ Upgrades for Run II", Ann. Rev. Nucl. Part. Sci. **50**, 71 (2000).
[5] R. Brun *et al* CERN-DD-78-2-REV
[6] T. Sjöstrand *et al* Computer Physics Commun. **135**, 238 (2001)
[7] J. Pumplin *et al*, J.H.E.P. **207**, 012 (2002)
[8] G. Corcella *et al*, J.H.E.P. **101** 010 (2001)
[9] S. Frixione and B.R. Weber, J.H.E.P. **206** 029 (2002)
S. Frixione, P. Nason and B.R. Weber, J.H.E.P. **308** 007 (2003)
[10] C.R. Hamberg, W.L. van Neerven and T. Matsuura, Nucl. Phys. **B359**, 343 (1991)
[11] D. Acosta *et al*, hep-ex/0406078, submitted to P. R. L.
[12] During runs with high instantaneous luminosities the di-muon trigger, as described below was pre-scaled. Instead an OR of three triggers, based on this trigger, but with additional requirements was used. As the OR of these triggers was found to be 100% efficient with respect to the basic di-muon trigger they are not treated separately.